Journal of Management & Entrepreneurship
ISSN 2229-5348

UGC Care Group I Journal
Vol-12 Issue-01 Jan 2023

Influence of heat treatments in H_2 and Ar on the E_1 center in β-Ga_2O_3

Mr. B. Srinidhi, Mrs. B. Santhoshi, Mrs. P. Kiranmayi, Mrs. G. R.V.A.Sushma,

Associate Professor, HOD[1,2], Assistant Professor[3], Assistant Professor[4]

KGRL COLLEGE (A) PG COURSES, BHIMAVARAM.

ABSTRACT

We looked at the possibility of the defect level E1 in heat treated n-type bulk β-Ga2O3 in hydrogen (H2) and argon (Ar) gases. The presence of hydrogen (H) doped β-Ga2O3 during H2 annealing at 900 °C has been verified via the use of Fourier transform-infrared spectroscopy. Studies using deep-level transient spectroscopy reveal that the addition of H increases the concentration of the E1 level, which contradicts the results seen in samples heat-treated in an Ar flow. Regardless of the presence or absence of a reverse-bias voltage, the E1 level does not change after heat treatments at 650 K. Possible causes of E1's flaw may be investigated using the hybrid-functional computations. We find three types of hydrogen-containing defect complexes that are consistent with E1 in terms of their charge-state transition levels. These include arrangements of singly hydrogenated Ga-O vacancies, shallow Ga-substitutional hydrogen-passivated donor impurities, and substitutional hydrogen at one of the triple coordinated O sites. The observed thermal stability of E1 is compatible with only the second kind of hydrogen binding energies.

• INTRODUCTION

In the presence of hydrogen, n-type materials are likely to create gallium vacancies (VGa) complexed with oxygen, according to ultra-wide computational investigations on monoclinic gallium sesquioxide (β-Ga O).

It is anticipated that semiconductors with a promising bandgap (Eg = 4.9 eV 2 31-3) would display substantial amounts of defects.33,43 Not to mention a for use in ultraviolet (UV) photodetectors and power electronics.4–9 To ensure that β-Ga O achieves its full potential, it is crucial to limit the amount of reports suggesting that H is linked to shallow donor states, which might be caused by the development of interstitial

1 - Hydrogen (H) or Hydrogen replacing oxygen (O) (H).45 Quite a few other H-related the material's imperfections that are electrically active, since these faults have a very important function as dopants or compensating centres in deciding the electrical conductivity of a semiconductor.10 Moreover, flaws in β-Ga2O3-based devices might affect their functioning via mechanisms such as binding the Fermi level 11–13 or serving as centres for recombination.14 As a result, β-Ga O defect levels have been extensively researched utilising methods like electron paramagnetic analysis.35, 39, 46–48

In as-received bulk crystals grown by edge-defined film-fed growth (EFG) and the Czochralski (CZ) method, as well as in epitaxial layers grown by molecular beam epitaxy (MBE)49 and halide vapour growth, the E1 centre is a DLTS defect signature with an activation energy of approximately 0.6 eV.

2, 3, and 23

methods such as steady-state phase epitaxy (HVPE), cathodoluminescence, magnetic resonance imaging (MRI), and others.An uptick in the reported by Polyakov et al.

DLTS, photo-capacitance, and other related techniques (20-30).1, 2, 4, 26, 31, and 36

There has been a lot of focus on H-related flaws in β-Ga2O3 as of late.pages 37–41 While Irmscher et al. demonstrated that a high-temperature heat treatment in an oxygen environment did not enhance the concentration of E1 in CZ-grown bulk crystals, experimental evidence suggests that EFG-grown bulk crystals with a surface orientation of (010) can be exposed to an H-plasma.31

The impact of radiation on the E1 level has been the subject of conflicting findings. Since the E1 concentration in EFG-grown bulk crystals remained unchanged after 0.6 and 1.9 MeV proton and neutron irradiation, respectively, Ingebrigtsen et al. and Farzana et al. concluded that E1 is not purely attributable to inherent flaws. Specifically, after subjecting HVPE sheets to 20 MeV proton irradiation, 18 MeV α-particle irradiation, and pulsed fast reactor neutron

irradiation, Polyakov et al. observed a small rise in the E1 concentration.

Ga

In this study, we detail how annealing with H2 and Ar affected the E1 level in bulk β-Ga2O3 crystals generated by EFG. Fourier transform-infrared spectroscopy (FT-IR) observations validate the incorporation of hydrogen into the crystals by annealing in H2, revealing an O-H vibrational line that was previously associated with a doubly hydrogenated Ga vacancy (Vib 2H).42 We discover that H2 heat treatments at 900 °C boost the concentration of E1 from DLTS measurements, but that comparable heat treatments in an inert Ar flow do not produce any discernible changes in the E1 concentration. H2 heat treatments do not affect the charge-carrier concentration, as we have discovered. We found that the E1 centre is stable at 650 K annealing conditions with and without an applied reverse-bias voltage. We conclude by comparing our findings with hybrid-functional calculations conducted on H-related defects in β-Ga2O3 and discussing possible sources of the E1 center's faults.

- METHODS

—

Two separate 0.7 mm thick wafers from distinct manufacturing batches were bought from Tamura Corporation, together with bulk EFG-grown β-Ga2O3 crystals52,53 with a surface orientation of (201). Both of the wafers were n-type doped inadvertently. Using a laser cutter, the wafers were divided into samples with dimensions of around ×5 5 mm2.

Heat treatments were applied to a subset of the samples in sealed quartz ampoules containing about half a bar of hydrogen gas at ambient temperature. Before the ampoules were filled with H2, a roughing pump was used to remove the samples from within. In particular, the ampoule was filled with 0.5 bar of H2 after three cycles of evacuation and refill with the gas, and then sealed. The heat treatments were carried out in a tube furnace set at 900 °C for an annealing period (tann) ranging from 15 to 75 minutes. The ampoule holding the sample was placed into the tube furnace after the temperature was established. After the necessary amount of time had elapsed, it was withdrawn from the furnace to cool down. After the samples had cooled to room temperature, they were taken out of the ampoules; in other words, they were not exposed to air at high temperatures. Also, three samples were heated in an Ar flow at 900 °C for 15–60 minutes, maintaining a constant temperature.

Infrared absorbance spectra were recorded at 5 K on as-received, H2-annealed, and Ar-annealed materials using Fourier transform infrared spectroscopy. A Bruker IFS 125HR spectrometer with a KBr beam splitter, an InSb detector, and a globar light source was used to conduct the tests. Samples were chilled in a Janis PTSHI-950-5 cryostat with ZnSe windows and He exchange gas using a closed-cycle, low vibration pulse tube design. The spectral resolution of all the observations was 0.5 cm−1, and the unpolarized light that hit the crystals came from a direction normal to their surface. For comparison, we referred to the empty sample holder's single-channel spectrum. The equation A log10 Tr was used to convert the recorded transmittance (Tr) data to absorbance (A).55

Samples were prepared in either their as-received or post-H2/Ar annealed states and then electrically characterised using Schottky barrier diodes (SBDs). A shadow mask and e-beam evaporation were used to deposit circular Ni pads with diameters ranging from 300 to 900 μm.33, 56, 32 The standard was 150 nm for the contact thickness. Ohmic contacts covering the back side of the samples were stacks of 10 nm thick Ti and 150 nm thick Al.

To make sure the SBDs were good for DLTS, we measured their current-voltage (IV) and capacitance-voltage (CV) in the dark. A Keithley 6487 picoammeter/voltage source was used for IV measurements, while a Boonton 7200 capacitance metre or an HP 4280A capacitance metre were used for CV measurements. The samples' donor concentration (ND) was calculated using CV measurements with a probing frequency of 1 MHz, supposing a static dielectric constant of 10.2.57. Additionally, the CV measurements were used to determine the probing depths for DLTS measurements, which in turn were based on the widths of the space-charge area (W).10

May 21, 2024 at 16:37:10

Two setups, both improved versions of the one detailed in Ref. 58, were used to conduct DLTS measurements spanning the temperature range of 150 to 700 K. To create the DLTS spectra, a GS2 filter, also known as a lock-in filter, was used.59 The 2NDΔC=Crb notation is used to illustrate the spectra, where ΔC is the amplitude of the capacitance transient observed in DLTS and Crb is the quiescent capacitance of the SBD at the reverse-bias voltage of application.10,60 By comparing the recorded DLTS spectra with simulations using a script based on Python, we were able to extract parameters that describe the electron traps seen in DLTS observations. These parameters include the trap concentration (Nt), the activation energy (EA), and the apparent capture cross section (σna).20 Nt was calculated here by factoring in the λ-correction.10, 20, and 31 It is anticipated that the error in σna will be within one order of magnitude, whereas the uncertainty in EA is projected to be around 0.04 eV.35

The 60-minute H2-annealed sample underwent thermal treatments to determine the E1 center's stability. The two methods used for conducting the annealing, reverse-bias annealing (RBA) and zero-bias annealing (ZBA), were respectively up to 650 K and with and without an applied reverse-bias voltage of -5 V. Following the steps outlined in Reference 36, the annealing cycles were executed with the exception of using a slower heating rate of 5 K/min and a voltage source provided by an HP 4280A capacitance metre.

In order to do first-principles calculations, the algorithms used in the VASP code were the projector augmented wave technique (61.62) and the Heyd-Scuseria-Ernzerhof (HSE) 64 screens hybrid functional.64 We modified the proportion of screened Hartree-Fock exchange to 33% and included the Ga 3d electrons in the valence. This leads to lattice parameters (a 12:23 Å, b 3:03 Å, c 5:79 Å, and β 103:8◦) that are in excellent agreement with experimental data, and a direct bandgap value of 4.9 eV.1.65% of the defects were calculated using 160-atom supercells and a 400 eV plane-wave cutoff.

has one unique k-point located at (0.25, 0.25, 0.25). With finite-size corrections made for charged defects, the approach provided in Ref. 66 was used to analyse the defect formation energies and thermodynamic charge-state transition levels.From 67 to 69 To determine the binding energies of H-related defect complexes, which were determined in accordance with first-principles calculations,42 we subtracted the formation energies of Hi and the remaining entity from the complex's formation energy while one H was annealed.33,43 The lack of this absorbance signature in the as-received and Ar-annealed samples (FT-IR data for Ar-annealed samples are not presented) suggests that Vib 2H is present in most of these samples in very low concentrations. In order to calculate the integrated absorbance of the feature associated with the LVM of Vib 2H, the data were modelled using Ga Lorentzian profiles. The total absorption is

The facility was evacuated by Ga.66 It is indicated by a positive binding energy that a~ib

steady compound.

We have constructed one-dimensional configuration coordinate (CC) diagrams illustrating the kinetics of the electron capture and emission process to allow comparison between the hybrid-functional calculations and EA derived for E1 from DLTS data.The hybrid-functional calculations were used to derive 70-72 CC model parameters, such as the ionisation energy (Ei), the change in the configuration coordinate (ΔQ), and the ground. These parameters are directly proportional to the concentration of VGa2H in the bulk crystals. Consequently, as shown in the inset of Figure 1, there is an approximately linear relationship between the Vib 2H Ga concentration and tann. Hence, during H2 annealing, the data shown in Fig. 1 demonstrate that H diffuses into the bulk of β-Ga2O3. Although secondary ion mass spectrometry and other chemical methods may theoretically detect H, the concentration is just too low. Keep in mind that the baseline noise is responsible for the tiny shoulder seen at 3439.5 cm−1 in Figure 1.

feeling elated Transfers between Franck-Condon (dFC and dFC). From SBDs that included as-received, EA retrieved IV and CV measures.

In addition to Ei, DLTS also incorporates an energy barrier for electron capture (Eb). The point where the ground and excited state potential energy curves connect is where the CC model derives this barrier.71

- RESULTS AND DISCUSSION
- Incorporation of hydrogen and electrical properties

Both the as-received and H2-annealed samples have their IR absorbance spectra adjusted for baseline in Figure 1. Free charge-carrier absorption, scattering at the rough back surface, and surface reflection losses all contribute to the baseline in the absorbance spectra.42 A localised vibrational mode (LVM) linked to Vib 2H is connected to an absorbance characteristic seen in the materials annealed in H2 at around 3437 cm−1.42 It is true that Vib 2H has alreadyThe SBDs demonstrated their suitability for conducting DLTS measurements in materials that were annealed with either H2 or Ar. Compared to samples that were either as-received or Ar-annealed, SBDs made on H2-annealed samples exhibited a greater leakage current in IV tests. Thus, the amount of tann that could be used for the H2 heat treatments was limited. The roughening of the sample surface during the H2 annealing process might be the cause of the increase in leakage current.23,50 on May 21, 2024 at 16:37:10

All samples, regardless of heat treatment, had ND values between 2 × 1017 and 5 × 1017 cm−3 as determined by CV measurements. All samples studied had Fermi levels near to EC, according to the ND values. The usual probing depth for DLTS measurements is found to be between 150 and 250 nm based on CV measurements. The H2 and the ND groups did not show any correlation with tann. What the hey! been discovered to develop under n-type circumstances during H2

Ar annealing. However, the as-received samples displayed a consid-

—

—

erable spread in N_D, and hence, a possible correlation between t_{ann} and N_D might be masked. Previously, Polyakov *et al.* have shown that surface treatments with H-plasma lead to an increase in carrier concentration for EFG-grown bulk crystals with a (201) surface orientation, which the authors proposed to be related to the forma- tion of shallow H-related donors.[50] Interestingly, H-plasma treat- ments caused a decrease in carrier concentration for EFG-grown bulk crystals with a (010) surface orientation.[38,50] This might be a result of distinct surface terminations on the (201) and (010) surfaces resulting from H treatment that influence the surface band bending.[41] It has also been shown that H can contribute to the unintentional doping found in as-grown bulk crystals.[40]

- E_1 concentration and stability

¼ ~ ×

DLTS spectra recorded on as-received, 30 min H_2-annealed, and 30 min Ar-annealed crystals are presented in Fig. 2. The E_1peak (E_A 0:60 + 0:04 eV, σ_{na} 6 10^{-13} cm^2) is present in all three spectra (see the inset in Fig. 2 to discern the peak for the as-received and Ar-annealed sample). At temperatures of around 280 K, the onset of a signature commonly labeled as E_2 can beseen, which has previously been shown to be related to substitu- tional Fe at tetrahedral Ga1 and octahedral Ga2 sites (Fe_{Ga1} and

Fe_{Ga2}

).[20,32,35] Notably, we did not observe the center commonly

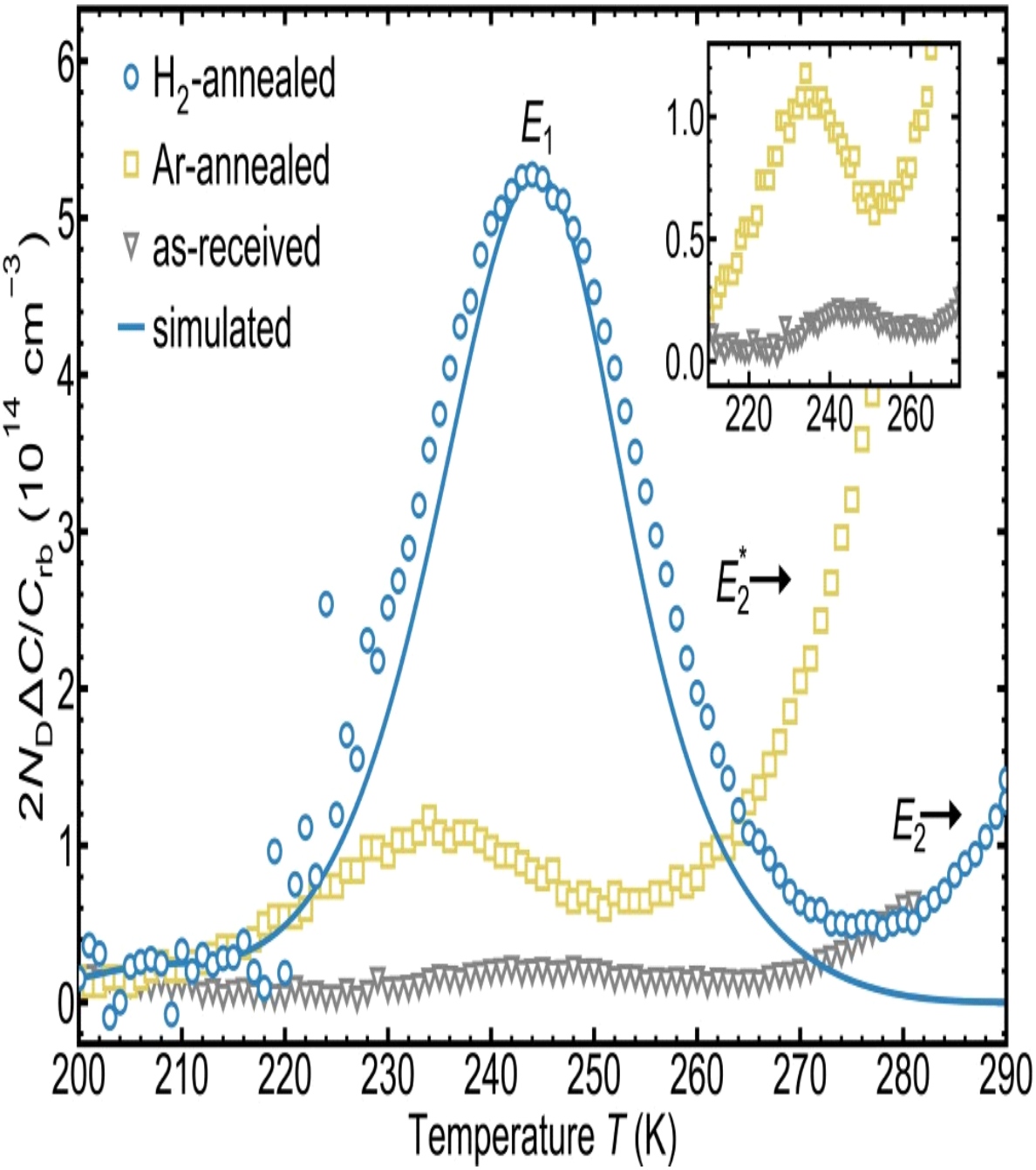
H2-annealed
Ar-annealed
as-received
simulated
E1
E2*
E2
2NDΔC/Crb (10^14 cm^-3)
Temperature T (K)
200
210
220
230
240
250
260
270
280
290
0
1
2
3
4
5
6
0.0
0.5
1.0
220
240
260

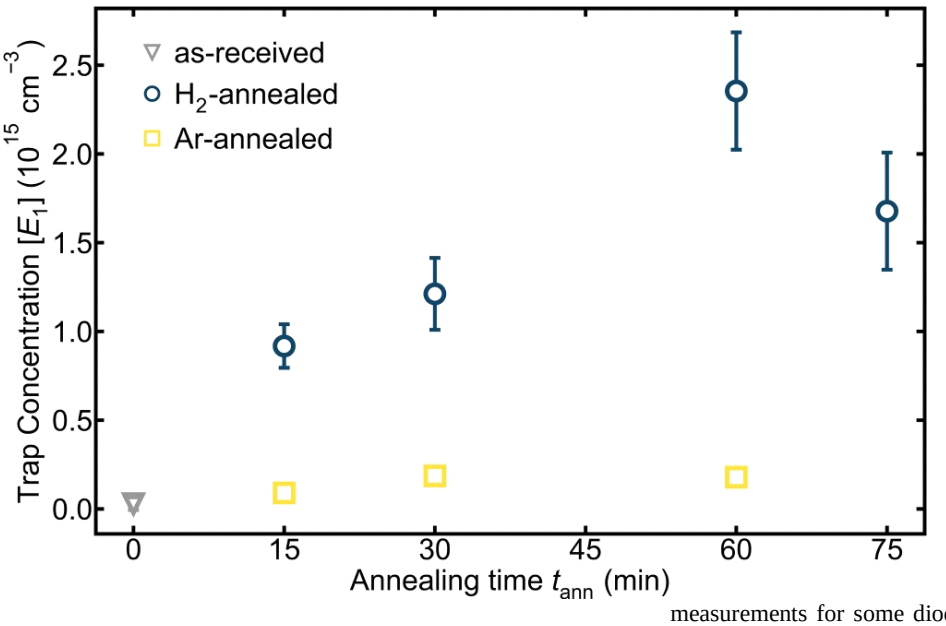

FIGURE 2. DLTS spectra captured on β-Ga2O3 bulk crystals formed using EFG either as-received, after H2 annealing, or after Ar annealing. A rate window of (640 ms)—1 is in use. A simulation is used to simulate the data for the H2-annealed sample, which is shown by the circles. We conducted the Ar anneal and the H2 anneal at 900 °C for 30 minutes each. There are labels on the observed flaw signatures. The E1 peak for both the as-received and Ar-annealed samples is shown in the inset. The inset plot's axis units match those of the main plot exactly.Figure 3 shows the average and standard deviation of the E1 concentration ([E1]) derived from DLTS measurements on bulk crystals formed using EFG as-received, H2-, and Ar-annealed methods, with respect to tann. [E1] was computed after considering the λ-correction.

following the anneal of H2 is denoted as E*.11,23,32,33, and 36 On the other hand, about 260 K in Fig. 2 you can observe the beginning of a tiny shoulder on the low-temperature side of E2 that represents a defect level around E* during Ar anneals.

In the spectra shown in Figure 2, the E1 level concentration is similar for the samples that were received and those that were annealed in Ar, but it is much greater for the sample that was annealed in H2. It should be noted that the Ar-annealed sample has a DLTS signature peak that is located at lower temperatures than the E1 level. This might mean that additional defect levels with comparable energy levels are formed during Ar annealing. The simulated line also shows that E1's DLTS signature (Fig. 2) is wider than what would be anticipated from a single level. As a result, we can't rule out the possibility that E1 has many layers that overlap. Using the high-resolution weighting algorithm GS4, however, we failed to discern a more intricate structure in the E1 peak.59 Multiple DLTS measurements were taken on as-received, Ar-annealed, and H2-annealed samples, and the E1 concentration as a function of tann is shown in Figure 3. Several diodes (ranging from 3 to 14) are used to determine the mean and standard deviation values for the as-received and H2-annealed samples, with the latter being used to check for lateral inhomogeneity, for the various tann. It should be noted that the 75-minute H2 annealing was carried out on a separate wafer, whereas the 15- and 60-minute annealing were done on a single wafer.

Figure 3 shows that the average E1 concentration in the bulk crystals when they are received is rather low. The E1 concentration was not detected in the DLTS measurements for some diodes on the as-received bulk crystals since it was below the detection limit of about 5 × 10−12 cm−3. The diodes on the samples that were received with E1 had a Nt of about 5 × 10^4 cm−3, when the λ-correction was included. The argon-annealed samples also showed a low E1 concentration of around 1×1014 cm−3. The E1 concentration does not systematically rise with increasing tann in the Ar-annealed samples either. The computed concentrations might be seen as an upper limit for the Ar-annealed samples since the E1 concentration was retrieved by considering the shifted peaks as belonging to E1. In contrast, the samples that were annealed in H2 show a much higher concentration of E1 in the range of 1 × 10– cubic centimetres. As the annealing duration rises, the mean E1 concentration does as well, up to and including 60 minutes.

The concentration of E1 is somewhat lower for the 75-minute annealed sample compared to the 60-minute ones, but it is still much higher than the as-received. Several defect processes may impact the total E1 concentration over lengthy annealing durations, as this suggests. Also, since the 60- and 75-minute annealed diodes are made from separate wafers, there may be some variation in the E1 concentration due to changes in the relative and absolute defect concentrations at the outset. Figures 2 and 3 show the findings, which we interpret as suggesting that E1 is linked to a defect related to H.2

Defects may be better identified by probing the stability of defect levels with respect to temperature and field. Using RBA and ZBA, it has been shown that many defect levels in β-Ga2O3 are metastable before (36,49). As an example, our prior work has shown that E* generated via H implanta-tion may be reversibly introduced and withdrawn at temperatures about 650 K by performing RBA and ZBA, respectively.36 Image 4 shows the results for the E_1 level following RBA and ZBA cycles. More specifically, DLTS spectra recorded after 60 min H_2 annealing and after subsequent RBA and

ZBA at 650 K are presented. A notable finding is that the peak intensity shows an insignificant change after the annealing cycles. The unchanged intensity suggeststhat E_1 is related to a stable defect. We observe only a slight

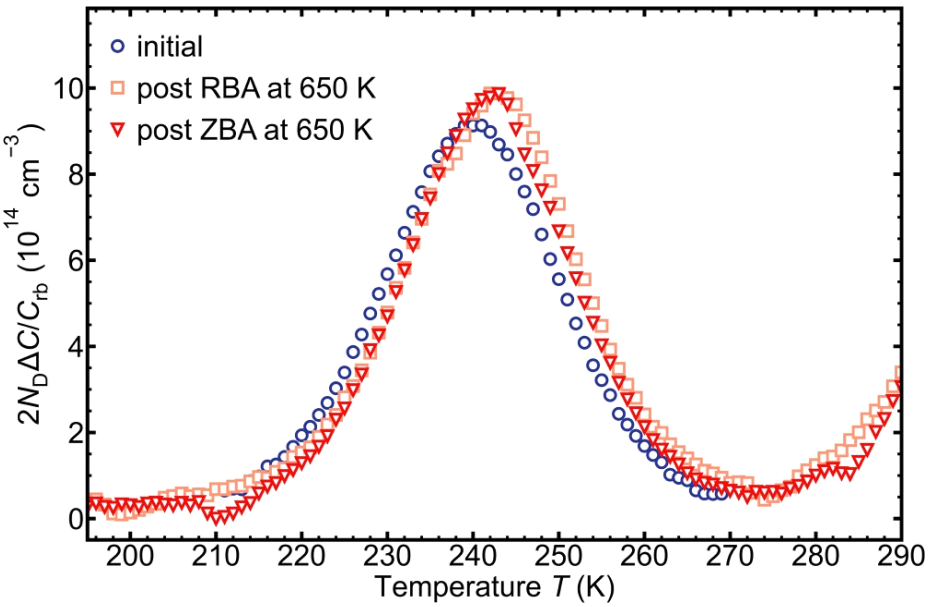

FIG. 4. DLTS spectra recorded on a sample annealed in H_2 for a duration of 60 min. The initial DLTS spectra and the DLTS spectra following RBA and ZBAat 650 K are shown. The rate window is $(640ms)^{-1}$.

increase (decrease) in the peak intensity (temperature position) of the E_2 signature, following RBA and no further change following ZBA. Furthermore, no distinct shoulder, which would correspond to E^* , emerges on the low-temperature side of E_2 after RBA at 650 K.

- Results of first-principles calculations

Assuming the E1 centre originated from an H-related source, hybrid-functional computations were carried out to investigate possible faults. Based on earlier computations, Hi only acts as a shallow donor in β-Ga2O3, as the expected ε(=) level is around EC.45 We also discover that electrically inactive and stable only in n-type material with a maximum binding energy of 0.85 eV, isolated hydrogen may also exist as interstitial molecular hydrogen (H2)i. On the other hand, Hi and (H2)i should be quite mobile.45 In fact, we determine migration barriers along the b-axis of 0.24 eV for Hi and 0.61 eV for (H2)i, respectively, using the climbing-image nudged elastic band method73 and the highly restricted and suitably normed semilocal functional,74. It is quite probable that H is present in a trapped form, such a defect complex including an inherent defect or maybe another impurity; β-Ga2O3 crystals formed by EFG often include Si, Al, Fe, and Ir.33.25 * þ

The formation and binding energy diagrams of several H-related defect complexes with charge-state transition levels at E1 are shown in Figure 5(a) and 5(b), respectively, and will be explored further on. There is another source that reports the production energies of the various faults listed below.Numbers 33–77 The error symbols are defined according to the reference 77.

We begin by thinking about inherent flaws that have the potential to trap

H. A HO complex that acts as a shallow donor may be produced by VO, as shown in earlier computations, by trapping H.45 Notably, as shown in Figure 5, the HO2 structure may also be stabilised at Fermi-level positions around EC in the single-negative charge state. Fig. 6 shows that in the single-negative charge state, there is a major structural rearrangement. In this state, two electrons are trapped in a localised state, and H transfers off the unoccupied triple coordinated O2 site to connect with the nearby Ga2 atom. Thermodynamic charge-state transitions from single positive to single negative are shown directly in Fig. 5(a), meaning that charge-neutral HO2 is unstable at any Fermi level and exhibits negative-U behaviour. The typical DLTS spectrum will show a peak at the emission of two electrons for a negative-U centre, but EA will be

found by the first emission of an electron, which corresponds to the ε(0=—) threshold for H.O. 79

2

The comparable Ei value for HO2 is around 0.68 eV, as seen in Table I, with a modest Eb of 0.10 eV. This value

is very similar to the observed EA for E1, which is 0.6 eV. Figure 5(b) shows that when the Fermi-level is close to EC, HO2 is predicted to exhibit poor thermal stability, with a maximum binding energy of 0.69 eV.

Table I shows the parameters of the CC model that were calculated for the nonradiative emission of an electron from several defect complexes involving H and EC, including Ei, Eb, dg, de, and ΔQ.This, together with the fact that the Hi migration barrier is low, suggests that HO2 should dissociate quickly.33 That doesn't seem to fit with E1 seeming stable on ZBA and RBA up to 650 KGa It is quite probable that Hi, in its role as a donor, would create stable complexes with acceptors like VGa.33,80 It is true that Vib 2H is responsible for the major O-H vibrational line seen by FT-IR in the hydrogen-annealed material.42 Complexation with H tends to move these levels further down to Fermi-level locations, however the predicted thermodynamic charge-state transition levels of VGa are more than 1.8 eV below EC.33

V V, or Ga-O divacancies, are another potential candidate.

• Football Club • Ga Odeon

Issue and change Ei (eV) Eb [eV] dg=e (eV) ΔQ (amu1/2̄) reveal levels of negative-U ε(=3) in the top portion of the bandgap, which are linked to the creation of Ga-Ga

Many crystal-forming reactions may include FC HO2 at VO.33,77 VGaVO, which can be expressed as 0.68, 0.10, 1.45 / 1.53, and 2.78.

The value of vib H-VO1 is 0.52−0.19−1.48 / 2.01−5.59.lographically incompatible arrangements.But although the

The Ga function is defined as VGa1H-VO1(−/2−).The negative-U charge-state transition levels tend to cluster around 0.49, 0.20, 1.46 / 2.03, and 6.41.

The value of SiGa1H (+/0) must be less than or equal to 0.99.

≤1.07 for SnGa2H (+/0) and all values thereafteraccording to the mix of tetrahedral Ga1 and octahedral Ga2 in the(i) move to lower Fermi-level locations when VGaVO dimer

Hydrogenation is performed on 2—Ga—Ga.77 We have already covered some of the possible E* centre defect origin configurations using the solitary and doubly hydrogenated VGaVO.77 Figure 5 shows that the pair of singly hydrogenated vacancies, Vib H-VO1 and VGa1H-VO1, have ε(0=2) levels around EC and E1. There are four other configurations in Reference 77 with comparable level positions, but they are not considered here since they have a higher energy. Figure 6 shows that the production of a Ga2-Ga2 dimer at VO1 is correlated with the 2-charge state. Here, ε(=2) is the important level to compare with DLTS, and the Ei (Eb) values for Vib H-VO1 and VGa1H-VO1, respectively, are 0.52 (0.19) and 0.49 (0.20) eV. E1 is also compatible with these energies.

Binding energies above 2.2 eV under n-type conditions are anticipated for Vib H-VO1 and VGa1H-VO1, in contrast to the HO2 complex, as seen in Figure 5(b). The 2.62 eV predicted for Vib 2H is similar to these binding energies.80 Moreover, this defect model is consistent with the idea that E1 might be made up of many overlapping defects, as there are multiple configurations of the singly hydrogenated diva-cancy that have identical activation energies.77

The VGa2H-VO2 and Via H-Vb con-type materials, as seen in Fig. 5(b), had binding energies of up to 0.58 eV for SiGa1H and 0.51 eV for SnGa2H, respectively. Furthermore, their stability is known to drop sharply as the Fermi level rises, suggesting that complex dissociation occurs in RBA settings. Even near the donor, Hiþ is favoured over H—i for lower Fermi-level locations. It is true that Fig. 5 displays 2þ charge states. correspond to a $H_i^{þ}$ immediately adjacent to $Si_{Ga}^{þ}$ or $Sn_{Ga}^{þ}$ (H forms a bond with the O indicated by arrows in Fig. 6). The single-

a positive electric field EC, the complex is in a comparable state, but with one electron in a delocalized disturbed host state66. Due to the inadequacy of the 160-atom super-cell for such spatially extended defect states, an exact assessment of ε(=0) cannot be made.84 If the donor ionisation energy is zero, as shown in Table I's upper estimates of 1 eV, then the ε(2 =) level is placed at EC. However, these donor complexes' incongruous low thermal and bias-induced stability cannot be reconciled with E1's.

• CONCLUSION

the complex is in a similar state, but with one electron in a delocalized disturbed host state66, due to a positive electric field EC. A precise evaluation of ε(=0) is not possible since the 160-atom super-cell is inadequate for such spatially wide defect states.84 As seen in the higher estimates of 1 eV in Table I, the ν(2 =) level is set at EC if the donor ionisation energy is zero. The poor temperature and bias-induced stability of these donor complexes, however, is incompatible with E1's.

REFERENCES

1In a 2011 publication by Janowitz et al., V. Scherer, M. Mohamed, A. Krapf, H. Dwelk, R. Manzke, Z. Galazka, R. Uecker, K. Irmscher, and R. Fornari, the authors published in the Journal of Physics, volume 13, issue 085014.

2With the help of T. Masui, T. Yamaguchi, K. Goto, S. Saito, K. Sasaki, T. Onuma, and T. Honda,

Appl. Phys. Lett. 108, 101904 (2016), with co-authors A. Kuramata and M. Higashiwaki.

3With contributions from T. Onuma, S. Saito, K. Sasaki, T. Masui, T. Yamaguchi, T. Honda, and M. Higashiwaki, this work was

published in Japan.The article was published in 2015 and can be accessed online at the following URLs: "https://doi.org/10.7567/JJAP.54.112601" in the Journal of Applied Physics, 54, 112601 in the Physical Sciences.
4M. Higashiwaki, K. Sasaki, H. Murakami, Y. Kumagai, A. Koukitu, A. Kuramata, T. Masui, and S. Yamakoshi, Semicond. HYPERLINK "https://doi.org/10.1088/0268-1242/31/3/034001" HYPERLINK "https://doi.org/10.1088/0268-1242/31/3/034001"Sci. HYPERLINK "https://doi.org/10.1088/0268-1242/31/3/034001" HYPERLINK "https://doi.org/10.1088/0268-1242/31/3/034001"Technol. 31, 034001 (2016).
5The authors of the article are S. Nakagomi, T. Momo, S. Takahashi, and Y. Kokubun. The article was published in the Physical Review Letters 103, 072105 in 2013.
6Y. Takahashi, S. Nakagomi, T. Sato, and Y. Kokubun, Sens. HYPERLINK "https://doi.org/10.1016/j.sna.2015.06.011" HTPERLINK ""Actuator HYPERLINK" https://doi.org/10.1016/j.sna.2015.06.011. " HYPERLINK " https://doi.org/10.1016/j.sna.2015.06.011."http://doi.org/10.1016/j.sna.2015.06.011 "A HYPERLINK ""HYPERLINK "https://doi.org/10.1016/j.sna.2015.06.011"Physical Review B 232, 208 (2015). 7.This is the ECS J. HYPERLINK "paper" by M. A. Mastro, A. Kuramata, J. Calkins, J. Kim, F. Ren, and S. Pearton."HYPERLINK "https://doi.org/10.1149/2.0031707jss" ""Solid HYPERLINK "https://doi.org/10.1149/2.0031707jss"HYPERLINK "https://doi.org/10.1149/2.0031707jss{"The article was published in the journal Science and Technology with the DOI: 10.11449/2.0031707jss. It is titled "State HYPERLINK "https://doi.org/10.1149/2.0031707jss" and was indexed in volume 6, page 356 in 2017.
8Z. Galazka, "Semicond. HYPERLINK "https://doi.org/10.1088/1361-6641/aadf78" Sci. HYPERLINK "https://doi.org/10.1088/1361-6641/aadf78" Techn. HYPERLINK "https://doi.org/10.1088/1361-6641/aadf78" 33, 113001 (2018).
9This is the application of the work of S. J. Pearton, J. Yang, P. H. Cary, F. Ren, J. Kim, M. J. Tadjer, and M. A. Mastro.in the journal Physical Review E, volume 10, issue 1, pages 11301–11302 (2018).
The Electrical Characterization of Semiconductors: Majority Carriers and Electron States, edited by P. Blood and J. Orton, published by Academic Press in 1992.
11J. F. Mcglone, Z. Xia, Y. Zhang, C. Joishi, S. Lodha, S. Rajan, S. A. Ringel, and A. R. Arehart, IEEE HYPERLINK "www.doi.org/10.1109/LED.2018.2843344" HYPERLINK ""Electron HYPERLINK" https://doi.org/10.1109/LED.2018.2843344" www.doi.org/10.1109/LED.2018.2843344" HYPERLINK "This is the link to the article: https://doi.org/10.1109/LED.2018.2843344. "Device HYPERLINK"www.doi.org/10.1109/LED.2018.2843344" HYPERLINK ""Lett. HYPERLINK "https://doi.org/10.1109/LED.2018.2843344 "38, 1042 (2018). Doi: 10.10109/LED.2018.2843344.
12J. F. McGlone, Z. Xia, C. Joishi, S. Lodha, S. Rajan, S. Ringel, and A. R. Arehart, "Appl. HYPERLINK "https://doi.org/10.1063/1.5118250" Phys. HYPERLINK "https://doi.org/10.1063/1.5118250" Lett. HYPERLINK "https://doi.org/10.1063/1.5118250" 115, 153501 (2019).
Citation: 13S.-S. Huang, R. Lopez, S. Paul, A. T. Neal, S. Mou, M.-P. Houng, and J. V. Li, Jpn,""HYPERLINK

"https://doi.org/10.7567/JJAP.57.091101""J. HYPERLINK "https://doi.org/10.7567/JJAP.57.091101" HYPERLINK "Physical Review A 57, 091101 (2018). 14In a 2017 publication by L. Huang, Q. Feng, G. Han, F. Li, X. Li, L. Fang, X. Xing, J. Zhang, and Y. Hao, the authors were published in the IEEE Photon journal. 15Along with M. E. Zvanut and S. Bhandari, J. HYPERLINK "This article was published in the following journals: "Appl. Phys. 127, 065704 (2020)" and "Chemistry & Physics 127, 1.5140193" (2020). 16In 2019, S. Bhandari, M. E. Zvanut, and J. B. Varley published an article in the following journals: Appl. Phys. 126, 165703; HYPERLINK "https://doi.org/10.1063/1.5124825" Physical Review E. 17The authors of this work are C. A. Lenyk, T. D. Gustafson, L. E. Halliburton, and N. C. Giles. The article was published in the Journal of Physical Science 126, 245701 in 2019. The authors of the article "18H. Gao, S. Muralidharan, N. Pronin, M. R. Karim, S. M. White, T. Asel, G. Foster, S. Krishnamoorthy, S. Rajan, L. R. Cao, M. Higashiwaki, H. von Wenckstern, M. Grundmann, H. Zhao, D. C. Look, and L. J. Brillson published it in the Physical Review Letters 112, 242102 in 2018. 19J. Phys. D: Appl. Phys. 53, 465102 (2020) by H. Gao, S. Muralidharan, M. R. Karim, S. M. White, L. R. Cao, K. Leedy, H. Zhao, D. C. Look, and L. J. Brillson. 20The authors of the article "New J. HYPERLINK " are C. Zimmermann, Y. K. Frodason, V. Rønning, J. B. Varley, and L. Vines."https://doi.org/10.1088/1367-2630/ab8e5b" HYPERLINK "The article is published in the Physical Journal B, volume 22, issue 063033 (2020). 21J. B. Varley, L. Vines, V. Bobal, Y. K. Frodason, C. Zimmermann, and V. Rønning published a paper in Phys.The article is published in the Physical Review Materials journal and has the DOI: https://doi.org/10.1103/PhysRevMaterials.4.074605"; it is indexed as Rev. HYPERLINK "https://doi.org/10.1103/PhysRevMaterials.4.074605"; and the page number is 074605. This was published in the Journal of Applied Physics by 22E. Farzana, E. Ahmadi, J. S. Speck, A. R. Arehart, and S. A. Ringel in 2018, volume 123, issue 161410. Section 23A. Y. J. Yang, E. B. Yakimov, I. V. Shchemerov, N. B. Polyakov, A. Kuramata, J. Kim, G. Yang, F. Ren, and S. J. Pearton, Appl. The article "Phys. "https://doi.org/10.1063/1.5012993" lets. (2018). HYPERLINK "https://doi.org/10.1063/1.5012993" 112, 032107.Part 24A. Y. S. J. Pearton, E. B. Yakimov, I. V. Shchemerov, N. B. Polyakov, A. Fares, P. B. Lagov, J. Kim, F. Ren, J. Yang, V. S. Stolbunov, and J. Kim are all authors. The Kochkova Appl. The article "Phys. HYPERLINK "https://doi.org/10.1063/1.5049130" Lett. 2018; 113: 092102 (HYPERLINK "https://doi.org/10.1063/1.5049130"). 25Z. A. R. Arehart, S. Zhang, E. Farzana, and A. The applicant is A. Ringel. In a recent publication in the “Phys. This is a link to a publication by Lett. "108, 052105 (2016)" HYPERLINK "https://doi.org/10.1063/1.4941429" Section 26A. Y. The authors of the paper are Polyakov, Smirnov, Gogova, Tarelkin, and Shchemerov. J. Pearton, J. HYPERLINK "https://doi.org/10.1063/1.5025916" AJR. This is from Physics, and the citation is as follows: Phys. (2018). 123, 115702 (HYPERLINK "https://doi.org/10.1063/1.5025916"). 27A. Okay. Y. I. V. Shchemerov, F. Ren, S. J. Pearton, N. B. Smirnov, and Polyakov Authors A. V. Chernykh and A. Kochkova, I., Appl. The article "Phys.